



HAL
open science

Self-assembly of tricuprous double helicates: Thermodynamics, kinetics, and mechanism

N. Fatin-Rouge, Sylvie Blanc, A. Pfeil, A. Rigault, A.-M. Albrecht-Gary,
J.-M. Lehn

► **To cite this version:**

N. Fatin-Rouge, Sylvie Blanc, A. Pfeil, A. Rigault, A.-M. Albrecht-Gary, et al.. Self-assembly of tricuprous double helicates: Thermodynamics, kinetics, and mechanism. *Helvetica Chimica Acta*, 2001, 84 (6), pp.1694-1711. 10.1002/1522-2675(20010613)84:63.0.CO;2-T . hal-01458136

HAL Id: hal-01458136

<https://hal.science/hal-01458136>

Submitted on 25 Apr 2024

HAL is a multi-disciplinary open access archive for the deposit and dissemination of scientific research documents, whether they are published or not. The documents may come from teaching and research institutions in France or abroad, or from public or private research centers.

L'archive ouverte pluridisciplinaire **HAL**, est destinée au dépôt et à la diffusion de documents scientifiques de niveau recherche, publiés ou non, émanant des établissements d'enseignement et de recherche français ou étrangers, des laboratoires publics ou privés.

Self-Assembly of Tricuprous Double Helicates: Thermodynamics, Kinetics and Mechanism

Nicolas Fatin-Rouge,[†] Sylvie Blanc,[†] Armin Pfeil,[‡] Annie Rigault,[‡] Anne-Marie Albrecht-Gary,^{†*} and Jean-Marie Lehn^{‡*}

Contribution from the Laboratoire de Physico-Chimie Bioinorganique, UMR 7509 du CNRS, Faculté de Chimie, 1 rue Blaise Pascal, 67000 Strasbourg, France, and the Laboratoire de Chimie Supramoléculaire, ISIS, Université Louis Pasteur, 4 rue Blaise Pascal, 67000 Strasbourg France.

**Submitted as an Article to
Helvetica Chimica Acta
Issue dedicated to Edgar Heilbronner**

[†] Laboratoire de Physico-Chimie Bioinorganique.

[‡] Laboratoire de Chimie Supramoléculaire.

* To whom correspondence should be addressed.

Abstract: We report in this paper the coordination and kinetic properties of two oligobipyridine strands containing three 2,2'-bipyridine subunits separated by 2-oxapropylene bridges, the CONEt₂ 4,4' disubstituted **L** and the CO₂Et 4,4' disubstituted **L'**. Spectrophotometric measurements allowed the characterization of thermodynamic complexes and kinetic intermediates* which are involved in the self-assembly process of **L**₂Cu₃ and **L'**₂Cu₃ helicates. The reaction presents positive cooperativity for the binding of two 2,2'-bipyridine strands to the cuprous cations. While reactive kinetic intermediates* present distorted coordination geometries around copper(I), the final rearrangement of the tricuprous bistranded helicates allows more closely tetrahedral coordination of each cation and reduces the interactions. Differences in the bulkiness and electronic properties of the **L** and **L'** substituents do not affect significantly the stability of the corresponding helicates, but greatly influence binding rates in the self-assembly process.

Keywords: Copper(I), helicates, 2,2'-bipyridine, self-assembly processes.

Introduction

In recent years, creating molecules that are programmed by virtue of their structure and binding sites to spontaneously organize themselves into supramolecular architectures held together by metal coordination has aroused the interest of chemists [1-5]. Using metal template strategy, helicates [6-16], ladder [17], grids [18], rings [2,3,19] cages [2,3,20], catenates and knots [21-23], were generated. In order to design such species presenting specific structural and functional features it is of great importance to establish the rules by which control the assembly process can be achieved through chemical programming by means of suitable components and assembling algorithms [1,5]. In the self-assembly of helicates, three main structural features determine the nature and shape of the helical species formed. The binding sites impose the number of strands able to coordinate metal ions with a given geometry. Bidentate or tridentate subunits combined respectively with metal ions of tetrahedral [6,7] and of octahedral ions [6,24] coordination geometry produce double helical polynuclear species while triple helical complexes are formed with bidentate ligands and octahedrally coordinated metal ions [25]. Taking into account these properties, double helical mixed valence [14] heteronuclear [26] or heterostranded [27] complexes have been synthesized. However not every combination of oligomultidentate ligands with metal ions will give helical structures and the spacers between the metal binding sites play an important role. They should be flexible enough to allow the ligand to bind strongly to the metal ion, and rigid enough to limit the number of conformations and favor interstrand over intrastrand binding. Finally, helicity implies that all metal centers must have the same screw sense and the same configuration at the metal centers. The family of double-stranded helicates generated from ligands with multiple diimine binding domains and transition metal ions of various binding geometries presents such properties. However, if their structures are well characterized by crystallography [6,7,28], NMR [6,7,29], mass spectroscopy [30,31] or

electrochemistry [32], few physico-chemical properties are available in the literature [33,34]. Spectrophotometric and thermodynamic parameters of triple helical lanthanide complexes have been reported [35]. Thermodynamic cooperativity was studied on double-stranded copper(I) [36] and silver(I) [37] trinuclear helicates. More recently, the stability constants of anchored triple ferric helicates in methanol have been determined [38]. The formation mechanism of such structures has been investigated [39,40], but further information on the parameters involved in the complexation process are required.

We report in this paper the coordination and kinetic properties of two oligobipyridine strands derived from the initial double helicate forming ligand [7] containing three 2,2'-bipyridine (bipy) subunits separated by 2-oxapropylene bridges, the CONEt_2 4,4' disubstituted **L** [41] and the CO_2Et 4,4' disubstituted **L'** [42] (*Fig. 1*). Using classical spectrophotometric titrations and electrospray mass spectrometric (ESMS) measurements, we have investigated the nature of the species that they form with copper(I) and determined their respective stability constants and absorption spectra in order to gain insight into the distribution of the different species at a given ligand/copper(I) ratio and into the physicochemical and mechanistic features of their self-assembly process. The formation kinetics of copper(I) complexes with **L** and **L'** have been investigated under the same experimental conditions by single and multiwavelength absorption spectrophotometry using fast mixing technique. A similar behaviour has been observed for both ligands, however the rate constants are very sensitive to structural changes.

Fig. 1

Experimental Section

Materials. Ligands **L** and **L'** were synthesized according to previously published procedures [41] and $[\text{Cu}(\text{CH}_3\text{CN})_4][\text{BF}_4]$ was prepared by the literature method [43]. The solvent selected for this work was a ternary mixture of solvents, acetonitrile/water/methylene

chloride (80/15/5 v/v), in which the ligands (CH_2Cl_2 , *Merck*, Uvasol), the copper salt (CH_3CN , *Merck*, Uvasol) and tetraethylammonium cyanide (water, *Fluka*), which was used for decomplexation studies, are soluble. The solvent was deaerated and protected from light. The ligand and cuprous stock solutions were prepared by accurate weighing. The ionic strength was fixed at 0.1 M with tetrabutylammonium trifluoromethanesulfonate (*Fluka*, puriss).

Electrospray Mass Spectrometric Measurements. ES mass spectra (*Fig. 2*) were obtained on a *VG BioQ* triple quadrupole with a mass to charge (m/z) range of 4000 (*VG BioTech Ltd*, Altrincham, UK). The ES interface was heated to 70 °C. The sampling cone voltage (V_c) was 20 V. No fragmentation process was observed at this voltage. The calibration was performed using multiprotonated ions from horse myoglobin. The resolution was about 600 at $m/z = 1000$ (with a valley of 10%) and then average masses were measured. Scanning was performed from $m/z = 400$ to 1400 in 10 s. The data system was operated as a multichannel analyzer, and several scans were summed to obtain the final spectra. Solutions containing the ligand **L** (1.2×10^{-4} M) and 0.2, 0.5, 1.0, 5.0, and 20.0 equivalents of copper(I) in $\text{CH}_3\text{CN}/\text{H}_2\text{O}/\text{CH}_2\text{Cl}_2$ (80/15/5) respectively were injected into the mass spectrometer source with a syringe pump (Harvard type 55 1111, *Harvard Apparatus Inc.*, South Natick, MA, USA) at a flow rate of 4 mL/min.

Fig. 2

Spectrophotometric Measurements. Titrations were carried out in 5 mL volumetric flasks using a precision piston microburet (*Gilmont*) to add copper(I) and the free ligand **L**. Between 18 and 24 solutions were prepared with a $[\text{Cu(I)}]_{\text{tot}}/[\text{ligand}]_{\text{tot}}$ ratio ranging between 0 and 1000. The ligand **L** concentration was first fixed at 1.2×10^{-4} M and copper(I) concentrations were varied between 0 and 2.4×10^{-3} M. The copper(I) concentration was then

fixed at 4.46×10^{-3} M and ligand concentrations were varied between 2.6×10^{-6} and 2.6×10^{-4} M. Another titration was done in excess of ligand **L** (6.7×10^{-4} M) with the cuprous concentrations varying between 6.9×10^{-6} M and 6.83×10^{-5} M. UV-vis (260-650 nm) absorption spectra were recorded on an Uvikon 941 (*Kontron*) spectrophotometer equipped with 0.2, 1 or 2 cm quartz cells (*Hellma*) and thermostated at 25.0 (1) °C. A typical set of spectra is given in *Fig. 3*.

Fig. 3

The spectrophotometric data were analyzed with both the *Letagrop-Spefo* [44-46] and *Specfit* [47-50] programs which adjust the absorbivities and the stability constants of the species formed at equilibrium. The *Letagrop-Spefo* program uses the *Newton-Raphson* algorithm to solve mass balance equations and a pit-mapping method to minimize the errors and determine the best parameter values. *Specfit* uses factor analysis to reduce the absorbance matrix and to extract the eigenvalue prior to the multiwavelength fit of the reduced data set according to the *Marquardt* algorithm [51,52].

Formation Kinetics of the Trinuclear Cuprous Helicates of L and L'. The reactions of copper(I) with ligands **L** and **L'** at 25.0 (1)°C involve rapid steps which were recorded on an *Applied Photophysic* stopped-flow SX-18MV spectrophotometer. Pseudo-first order conditions with respect to the ligands (2.5×10^{-5} M) were used and copper(I) concentrations were varied between 2.5×10^{-4} and 2×10^{-3} M. Experiments with excess of **L'** (1.449×10^{-4} M; 8.69×10^{-4} M; 5.80×10^{-4} M and 2.90×10^{-4} M) were also undertaken in $\text{CH}_3\text{CN}/\text{CH}_2\text{Cl}_2$ (80/20 v/v) using a low concentration of copper(I) (5.8×10^{-6} M). The data sets, averaged out of at least three replicates and recorded with a one cm path length at the absorption maximum of the LMCT band, were analyzed on-line with the commercial software *Biokine* [53]. This program fits up to three exponential functions to the experimental curves with the *Simplex*

algorithm [54] after initialization with the *Padé-Laplace* method [55]. The second-order rate constants were calculated by non-weighted linear regression using the commercial *Enzfitter* program [56] based on *Marquard* [51] analysis. Time-resolved absorption spectra were also collected between 300 and 450 nm with a one cm path length. The rate constants and the extinction coefficients were adjusted to the multiwavelength data sets by nonlinear least-squares analysis with the *Specfit* program [47-50].

Results

Thermodynamics and Spectrometry. The ESMS mass spectra recorded at various $[\text{Cu(I)}]_{\text{tot}} / [\text{L}]_{\text{tot}}$ ratios (*Fig. 2*) indicate the formation of four complexes: LCu , LCu_2 , L_2Cu_2 and L_2Cu_3 (see *Table SI*). They also reveal that the double helicate L_2Cu_3 is already the major product at a $[\text{Cu(I)}]_{\text{tot}}/[\text{L}]_{\text{tot}}$ ratio of 0.5, well below the stoichiometric value of 1.5.

Spectrophotometric titrations of **L** with copper(I) (*Fig. 3*) were carried out in order to calculate the binding constants of the complexes and to determine the corresponding electronic spectra (260-650 nm). The best fit of the spectrophotometric data was obtained by both *Specfit* [47-50] and *Letagrop-Spefo* [44-46] programs with a model including three complexes observed by ESMS (LCu , L_2Cu_2 and L_2Cu_3), LCu_2 having not been characterized under our experimental conditions. The values of the global stability constants obtained are summarized in *Table 1*.

Table 1

The absorption spectra of the copper(I) complexes are dominated by a ligand-to-metal charge transfer band (LMCT) in the visible region ($\lambda_{\text{max}} = 460\text{-}470$ nm). Using the stability constants presented in *Table 1*, the corresponding distribution curves were calculated with the *Haltafall* program [57]. *Fig. 4a* shows in agreement with the ESMS data the formation of the

trinuclear helicate L_2Cu_3 in competition with two minor cuprous complexes LCu and L_2Cu_2 . *Fig. 4b* and *Fig. 4c* correspond to the experimental conditions chosen for kinetic measurements in excess of copper(I) and in excess of ligand L' , respectively.

Fig. 4

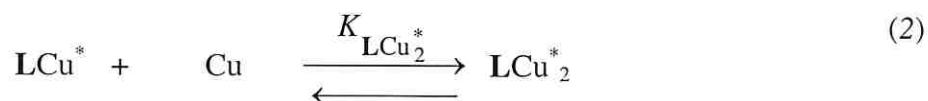
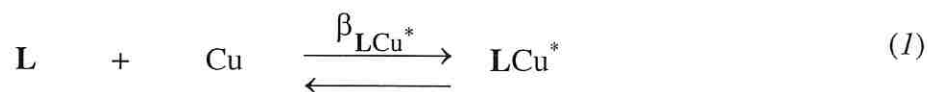
Formation Kinetics of L Cuprous Complexes. Kinetic measurements were carried out in an excess of copper(I) with respect to the concentration of L . A large loss of spectrophotometric amplitude (30% of the total amplitude) was observed during the dead time (3 ms) of the stopped-flow device. Under pseudo-first order conditions with respect to copper(I), three exponential spectrophotometric signals were recorded at 468 nm in the time range of seconds and minutes. For simplicity, the different steps are successively denoted 1, 2, 3 and 4, as indicated in *Fig. 5*. The values of the corresponding pseudo-first order rate constants $k_{2,obs}$, $k_{3,obs}$ and $k_{4,obs}$ were determined [53] and are presented in *Table S2*.

Fig. 5

Using a diode arrays device, we could confirm the three rate limiting steps. The most striking feature observed in *Fig. 6* is the presence of two absorption bands centered at about 380 nm and 560 nm. These bands were not observed at equilibrium (*Fig. 3*) and strongly suggest that reactive kinetic intermediates* are involved in the self-assembly process of L_2Cu_3 . For that reason all the cuprous species involved in the proposed mechanism are written with an asterisk.

Fig. 6

The variations of the absorbance $A_{1,\infty}$, measured at 468 nm and at the beginning of the second step, after the initial loss of spectrophotometric amplitude (*see Table S3*) versus the analytical concentrations in L and copper(I) suggest the rapid formation of two cuprous species with a single strand L in two successive reactions:

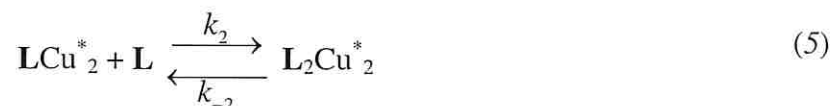


This reaction scheme leads to the following equations and to the determination of $\varepsilon_{\text{LCu}^*}$, β_{LCu^*} , $\varepsilon_{\text{LCu}_2^*}$ and $\beta_{\text{LCu}_2^*}$:

$$A_{2,0} = \varepsilon_{\text{LCu}^*} \times [\text{LCu}^*] + \varepsilon_{\text{LCu}_2^*} \times [\text{LCu}_2^*] \quad (3)$$

$$A_{1,\infty} = \frac{[\text{L}]_{\text{tot}} [\text{Cu}]_{\text{tot}}}{(1 + \beta_{\text{LCu}^*} [\text{Cu}]_{\text{tot}} + \beta_{\text{LCu}_2^*} [\text{Cu}]_{\text{tot}}^2)} \left(\beta_{\text{LCu}^*} \varepsilon_{\text{LCu}^*} + \beta_{\text{LCu}_2^*} \varepsilon_{\text{LCu}_2^*} [\text{Cu}]_{\text{tot}} \right) \quad (4)$$

In the second step, a decrease of the corresponding pseudo-first order rate constant $k_{2,\text{obs}}$ was observed when copper(I) concentrations increased. We propose that this step could involve the binding of a second strand to the dicuprous species LCu_2^* rapidly formed:



According to this reaction scheme, the expression of $k_{2,\text{obs}}$ can be written as:

$$k_{2,\text{obs}} = \frac{4 \times k_2 \times \beta_{\text{LCu}_2^*} \times [\text{L}]_{\text{tot}} \times [\text{Cu}]_{\text{tot}}^2}{(1 + \beta_{\text{LCu}^*} \times [\text{Cu}]_{\text{tot}} + \beta_{\text{LCu}_2^*} \times [\text{Cu}]_{\text{tot}}^2)^2} + k_{-2} \quad (6)$$

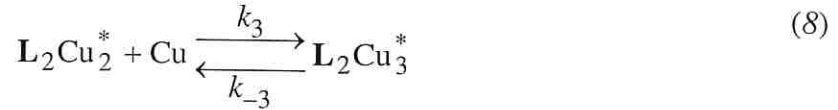
At the end of this second step the term $[\text{L}_2\text{Cu}_2^*]_{\infty} - [\text{L}_2\text{Cu}_2^*]^2$ was neglected.

The values of the rate constants k_2 and k_{-2} were determined by a non-linear least squares methods (Fig. 7a) and are given in Table 2. The variations of $A_{2,\infty}$ measured at 468 nm at the end of step 2 (eq. 7), are given in Table S3 and lead to the determination of $\varepsilon_{\text{L}_2\text{Cu}_2^*}$, $\beta_{\text{L}_2\text{Cu}_2^*}$ being equal to $(k_2/k_{-2}) \times \beta_{\text{LCu}_2^*}$.

$$A_{2,\infty} = \frac{[\text{L}]_{\text{tot}} \times [\text{Cu}]_{\text{tot}}}{(1 + \beta_{\text{LCu}^*} \times [\text{Cu}]_{\text{tot}} + \beta_{\text{LCu}_2^*} \times [\text{Cu}]_{\text{tot}}^2)} \times \left(\beta_{\text{LCu}^*} \times \varepsilon_{\text{LCu}^*} + \varepsilon_{\text{LCu}_2^*} \times \beta_{\text{LCu}_2^*} \times [\text{Cu}]_{\text{tot}} + \frac{\varepsilon_{\text{L}_2\text{Cu}_2^*} \times \beta_{\text{L}_2\text{Cu}_2^*} \times [\text{L}]_{\text{tot}} \times [\text{Cu}]_{\text{tot}}}{(1 + \beta_{\text{LCu}^*} \times [\text{Cu}]_{\text{tot}} + \beta_{\text{LCu}_2^*} \times [\text{Cu}]_{\text{tot}}^2)} \right) \quad (7)$$

Fig. 7

The variations of the observed rate constant $k_{3,obs}$ with the copper(I) concentration, suggest that a third cuprous cation binds to the dinuclear double stranded complex $L_2Cu_2^*$ during the third rate-limiting step:



The kinetic data fit well with the following equation which corresponds to the proposed mechanism (Fig. 7b) and leads to the determination of k_3 and k_{-3} (Table 2).

$$k_{3,obs} = \frac{4 \times k_3 \times \beta_{L_2Cu_2^*} \times [L]_{tot} \times [Cu]_{tot}^3}{\left(1 + \beta_{LCu^*} \times [Cu]_{tot} + \beta_{LCu_2^*} \times [Cu]_{tot}^2\right)^2} + k_{-3} \quad (9)$$

The fourth and slowest step can be considered as a final rearrangement of the trinuclear double stranded intermediate*:



The corresponding variations of the pseudo-first order rate constant $k_{4,obs}$ versus the analytical concentrations in **L** and in copper(I) are expressed by the following equation:

$$k_{4,obs} \approx \frac{4 \times k_4 \times \beta_{L_2Cu_3^*} \times [L]_{tot} \times [Cu]_{tot}^3}{\left(1 + \beta_{LCu^*} \times [Cu]_{tot} + \beta_{LCu_2^*} \times [Cu]_{tot}^2\right)^2} + k_{-4} \quad (11)$$

As for the other previous steps, the term $[L_2Cu_3^*]^2 - [L_2Cu_3^*]_{\infty}^2$ was neglected. A statistical treatment by a non-linear least squares method leads to the k_4 and k_{-4} values (Fig. 7c), which are presented in Table 2 with their standard deviations.

Table 2

Time-resolved absorption spectra were recorded from 350-700 nm. The set of spectra displayed in *Fig. 6* shows a maximum at 558 nm during the first stage, which undergoes a 100 nm blue shift during the following steps. Factor analysis of the entire spectrophotometric data set confirmed the presence of four absorbing species. A satisfactory least-squares fit of the apparent rate constants and absorptivities can be obtained with the previous scheme of successive reaction steps (1),(2),(5),(8),(10).

Formation Kinetics in Excess of L' Cuprous Complexes. Kinetic experiments were carried out for **L'** in excess of either copper(I) (*Table 3*) or ligand (see *Fig. S1*). The same mechanism as observed for **L** was found. The corresponding rate constants for each of the three rate-determining steps are given in *Table 2*.

Table 3

In excess of ligand **L'**, two monocuprous species **L'Cu** and **L'₂Cu** are formed at equilibrium as shown by the distribution curves (*Fig. 4*). A single exponential signal was observed at 500 nm. The corresponding pseudo-first order rate constant $k_{1,obs}$ varies linearly with the analytical concentration of **L'**. The values of the first and second-order rate constants, which correspond to the ordinate at the origin and to the slope of the line, are calculated by linear regression and are equal to $k_1 = 1.7 (6) \times 10^3 \text{ M}^{-1} \text{ s}^{-1}$ and $k_{-1} = 0.22 (5) \text{ s}^{-1}$, respectively (*Table 2*).

Discussion

Characterization of Cuprous Complexes of Ligands of L and L'. Depending on the ratio $[\text{Cu(I)}]_{\text{tot}}/[\text{L}]_{\text{tot}}$, three thermodynamic cuprous complexes, LCu , L_2Cu_2 and L_2Cu_3 , which are of the same stoichiometry as the species observed with L' in $\text{CH}_3\text{CN}/\text{H}_2\text{O}/\text{CH}_2\text{Cl}_2$ [36], were characterized in $\text{CH}_3\text{CN}/\text{H}_2\text{O}/\text{CH}_2\text{Cl}_2$ (80/15/5) by absorption spectrophotometry (*Fig. 3*) and ESMS (*Fig. 2*). In a large excess of copper(I), LCu_2 was detected by ESMS, but not by absorption spectrophotometry (*Fig. 2d*). The stability of the three cuprous L and L' complexes were characterized at equilibrium, the mononuclear monostranded complex and the dinuclear and trinuclear bistranded species (*Table 1*). For the sake of comparison, collected thermodynamic and spectrophotometric data for cuprous complexes formed with various bipy derivatives are presented in *Table 4*. The distribution curves in *Fig. 4a* and *Fig. 4b* show the highly favored formation of the L_2Cu_3 species, indicating appreciable positive cooperativity in agreement with the results obtained for $\text{L}'_2\text{Cu}_3$ [36].

Table 4

Ligands **2**, **4**, **5**, **6** and **8** were examined in the same solvent as L' . The stability constants of the monomeric cuprous complex with **4** (*Table 4*) and the corresponding $\text{L}'\text{Cu}$ species (*Table 1*) are identical within experimental errors. The same observation holds for the dimeric complexes with **4** and L' . These observations suggest that the formation of these two oligo-bipyridine cuprous complexes is not subject to increased steric hindrance compared to the corresponding species with the model ligand **4**. If we compare L and L' , no significant difference is observed in the stability of the cuprous complexes within experimental errors (*Table 1*). These data do not reflect that L is bearing bulkier substituents than L' or that 5% water was added to the solvent used for L .

The copper(I) complexes of bipy and its derivatives give a broad intense MLCT band ($d\pi \rightarrow \pi^*$) in the visible (430-530 nm), [58-60]. The λ_{max} and the absorbtivity of this band

strongly depend on the substituents attached to the bipy moiety [61], which affect the geometry of the cuprous complexes, the Cu-N bond length, and the electronic properties of the nitrogen atoms [61-63]. An electron-withdrawing substituent shifts the absorption band to a lower frequency, whereas an electron-donating substituent raises the frequency [64]. The steric bulk of the substituents may cause lengthening of the Cu-N bond, leading to the destabilization of metal complexes, resulting in a poor back-bonding, and a compensatory blue-shift of the MLCT maximum [64]. Taking into account the electronic effects of the (CO₂Et) and (CONEt₂) 4,4'-substituents as well as the effects of the steric bulk of these substituents, one may conclude that the differences in the spectrophotometric properties of the cuprous complexes of **8** and **L** are predominantly determined by steric effects, whereas both electronic and steric effects contribute when comparing the analogous complexes of **8** and **L'**. The electronic properties of the substituents could explain the observed blue shift of the MLCT bands of **L'** and **L** cuprous complexes, respectively (*Table 1* and *Table 4*).

The absorption spectra obtained for **LCu**, **L₂Cu₂** and **L₂Cu₃** clearly indicate the coordination of two bipy units to the copper centers. The only structure which can be proposed for **LCu** is therefore the coordination provided by a folded ligand **L**. The -CH₂OCH₂- is short enough to hinder tetrahedral binding of an ion by two consecutive bipy groups of the same ligand. We conclude that the copper(I) cation in **LCu** is coordinated by the two external bipy. Such a folded structure has already been observed for the copper(I) species formed with 2,2'-bis(6-(2,2'-bipyridyl)biphenyl) [65]. The two **L₂Cu₂** and **L₂Cu₃** species are expected to be of double helicate type by analogy with the tricuprous species of its unsubstituted parent **8**, for which the double helicate structure was confirmed by X-ray crystallography [7]. The X-ray structure [66] of **L'₂Cu₃** shows that the presence of the diethylester groups increases the stacking of the bipy groups and enhances the distortion of the tetrahedral coordination geometry compared to its unsubstituted analog. The variation of

the electronic maxima then indicates that the stacking of the bipy units decreases between L'_2Cu_3 and L_2Cu_3 . Moreover, the similarity of the stability constants related to L'_2Cu_2 and its corresponding analog with the ditopic ligand **6** (Table 4) in the same solvent could suggest that the structure of the two complexes is similar and that the two cuprous cations in L'_2Cu_2 occupy vicinal coordination sites. As a consequence the third cuprous cation would then coordinate to the free external binding sites (Fig. 8).

Fig. 8

Cuprous Complexes Formation Processes. The same formation process with four steps (Table 2) has been found for the formation of the tricuprous helicates L_2Cu_3 (Fig. 5) and L'_2Cu_3 (Table 3). Step 1 involving two copper(I) cations leads to the formation of LCu^* . These reactions were too fast to be measured by a stopped flow technique in agreement with the high values of the second order rate constant observed for the formation of the (bipy)Cu(I) or (6,6'(CH₃)bipy)Cu(I) complex (*ca* $10^8 M^{-1} s^{-1}$) [67]. Fig. 6 shows an intense absorption band centered at 560 nm in the time-resolved spectra and indicates the formation of kinetic intermediates* LCu^* and LCu^*_2 which do not have the same coordination geometry as the corresponding thermodynamic cuprous species, displaying a different spectrophotometric behaviour. A monomeric cuprous complex with an open chain N₄ Schiff base ligand (1,8-bis(2-pyridyl)-2,7-diazaoctadiene-1,7) presents a characterized. The spectrum of this species was characterized by two absorption maxima at approximately 420 and 600 nm in CH₃CN [68]. The data for ϵ_{max} , which are sensitive to the solvent, strongly suggest the participation of the solvent to the inner coordination sphere of copper(I). Two monomeric complexes combine in CH₃CN to form a binuclear helical complex, which allows an almost ideal tetrahedral coordination of each copper(I) [68]. These data suggest that in our process (Fig. 6) the first reactive intermediate* could have a highly distorted coordination geometry and that CH₃CN could participate to the inner coordination sphere.

The second step could be related to the addition of the second strand, which is two orders of magnitude lower than the second order rate constant measured for the formation of the (6,6'(CH₃)bipy)₂Cu(I) complex ($2.7 \times 10^7 \text{ M}^{-1} \text{ s}^{-1}$) [67]. Steric effects could explain these data. The rate constant is three times higher for **L** ($k_2 = 7 (2) \times 10^5 \text{ M}^{-1} \text{ s}^{-1}$) than for **L'** ($k_2 = 2.0 (5) \times 10^5 \text{ M}^{-1} \text{ s}^{-1}$). A slow binding of the second **L'** on **L'**Cu* was also observed in excess of ligand **L'** (Table 2). Step 2 is slower, when the bulkiness of the substituents decreases. This result suggests that bulky substituents could prevent early concerted rearrangement and favour the formation of more reactive intermediates* with distorted coordination geometries, which will facilitate the approach of a second strand. If we consider the back reaction, **L**₂Cu*₂ dissociates *ca* 100 times faster ($k_{-2} = 53.0 (4) \text{ s}^{-1}$) than **L'**₂Cu*₂ ($k_{-2} = 0.6 (1) \text{ s}^{-1}$). These data agree well with our previous discussion and confirm the higher reactivity of the kinetic intermediate* **L**₂Cu*₂ compared to **L'**₂Cu*₂.

Step 3 could be assigned to the complexation of the last copper(I) cation. The low rate constant values observed for the copper(I) coordination leading to **L**₂Cu₃*, $k_3 = 1.0 (1) \times 10^3 \text{ M}^{-1} \text{ s}^{-1}$ and $45 (9) \text{ M}^{-1} \text{ s}^{-1}$ for **L** and **L'** respectively, reflects the difficulty of the cation to reach the coordination site due to the geometric organization of the ligands imposed by the complexation of the two first copper(I). The difference between **L** and **L'** could also be due to the lower basicity of the bipy nitrogen sites of **L'** due to the stronger electron withdrawing effect of the ester group. The respective dissociation reactions of **L**₂Cu₃* and **L'**₂Cu₃* are of the same order of magnitude and do not reflect any significant effect of the substituents on these intermediate structures*.

The last monomolecular step, independent of copper(I) and of ligand concentration, is attributed to a final intracomplex rearrangement, which leads to the thermodynamic tricuprous helicates. The slow rearrangement rates are similar for **L**₂Cu₃* ($2 (2) \times 10^{-2} \text{ s}^{-1}$) and **L'**₂Cu₃* ($1.4 (2) \times 10^{-2} \text{ s}^{-1}$).

Our spectrophotometric results at equilibrium are dominated by the formation of bis(bipy) coordination sites around copper(I) with the expected absorbances related to tetrahedral geometries. This trend could even lead to folded structures as suggested earlier [39]. The self-assembly process of the helicates L_2Cu_3 and L'_2Cu_3 goes via intermediates* with highly distorted coordination geometries, clearly reflected by absorption bands at 560 nm, which lead to a slow and final rearrangement of the helicates. For ligand L' , the activation parameters were calculated for steps 2, 3 and 4 respectively ($\Delta S_2^\ddagger = 17$ eu, $\Delta H_2^\ddagger = 5.3$ kcal mol⁻¹, $\Delta G_2^\ddagger = 0.2$ kcal mol⁻¹; $\Delta S_3^\ddagger = 4$ eu, $\Delta H_3^\ddagger = 2.3$ kcal mol⁻¹, $\Delta G_3^\ddagger = 1.1$ kcal mol⁻¹; $\Delta S_4^\ddagger = 0.7$ eu, $\Delta H_4^\ddagger = 2.1$ kcal mol⁻¹, $\Delta G_4^\ddagger = 1.9$ kcal mol⁻¹). These data show a decreasing entropic contribution along the process and a high activation energy for the rearrangement of the helicate L'_2Cu_3 .

The mechanistic scheme is markedly complicated by the fact that the binding of two oligo-bipy strands with Cu(I) ions may yield both non-entangled "side-by-side" and helical structures [69]. One could expect the formation of the first type to be kinetically faster than that of the second where the ligands have to wrap around each other. Note also that stacking between the bipy subunits is only possible in the double helical form. Thus, one might suggest that the reactive kinetic intermediates* formed in the complexation process involve "side-by-side" type structures, with more or less distorted Cu(I) coordination sites, which would then rearrange to the thermodynamic, more stable, helical species. As a consequence, the last step occurring in a monomolecular fashion between species possessing both two strands and all three Cu(I) centers, would correspond to such an internal rearrangement to the final fully double helical complex. *Fig. 9* presents a partial schematic illustration of this highly complicated situation.

Fig. 9

Conclusion

The present study has allowed to unravel at least partially, the kinetic and mechanistic processes occurring on formation of double helicates. It shows that such self-assembly processes, following a directing program [1], may involve highly complex routes towards the final encoded thermodynamic entity.

When the reactions become slow enough, intermediates* may be stable enough for isolation and characterization, as was the case in the formation of circular helicates which is preceded by a kinetically favored triple helicate [70]. In a broader view, kinetic studies provide insight into the various steps and intermediates* of complex self-assembly processes, and therefore into the factors which influence the output entities. Such information is of much interest for progressively gaining control over the evolution of self-assembling systems by introducing suitable and robust instructions in the programming.

Acknowledgments. The authors thank Dr. A. Van Dorsselaer and Dr. E. Leize for the ESMS spectra.

Supporting Information Available: Table S1 listing ESMS Mass values, and Table S2, Table S3 and Figure S1 presenting kinetic data.

References

- [1] J.M. Lehn, *Supramolecular Chemistry: Concepts and Perspectives*, VCH: Weinheim, 1995, Chapter 9, p. 139.
- [2] For recent reviews on metal ion-mediated self-assembly, see for example: P. N. W. Baxter, in 'Comprehensive Supramolecular Chemistry', Eds. J. L. Atwood, J. E. D. Davies, D. D. MacNicol, F. Vögtle, J.-M. Lehn, Pergamon, Oxford, 1996, Vol.9, Chapter 5, p. 165; E. C. Constable, in 'Comprehensive Supramolecular Chemistry', Eds. J. L. Atwood, J. E. D. Davies, D. D. MacNicol, F. Vögtle, J.-M. Lehn, Pergamon, Oxford, 1996, Vol.9, Chapter 6, p. 213; M. Fujita, in 'Comprehensive Supramolecular Chemistry', Eds. J. L. Atwood, J. E. D. Davies, D. D. MacNicol, F. Vögtle, J.-M. Lehn, Pergamon, Oxford, 1996, Vol.9, Chapter 7, p. 253.
- [3] D. S. Lawrence, T. Jiang, M. Levett, *Chem. Rev.* **1995**, *95*, 2229; R. F. Saalfrank, *Curr. Opin. Solid State Mat. Sci.* **1998**, *3*, 407; B. Olenyuk, A. Fechtenkötter, P. J. Stang, *J. Chem. Soc. Dalton Trans.* **1998**, *11*, 1707; M. Fujita, *Polym. Mater. Sci. Eng.* **1999**, *80*, 27; D. L. Caulder, K. N. Raymond, *J. Chem. Soc. Dalton Trans.* **1999**, *8*, 1185; C. Piguet, *J. Inclusion Phenom. Macrocycl. Chem.* **1999**, *34*, 361. S. Leininger, B. Olenyuk, P. J. Stang, *Chem. Rev.* **2000**, *100*, 853; G. F. Swiegers, T. J. Malefetse, *Chem. Rev.* **2000**, *100*, 3483.
- [4] A. Williams, *Chem. Eur. J.* **1997**, *3*, 15.
- [5] J.-M. Lehn, *Chem. Eur. J.* **2000**, *6*, 2097.
- [6] C. Piguet, G. Bernardinelli, G. Hopfgartner, *Chem. Rev.* **1997**, *97*, 2005; E.C. Constable, *Tetrahedron* **1992**, *48*, 10013.
- [7] J.M. Lehn, A. Rigault, J. Siegel, J. Harrowfield, B. Chevrier, D. Moras, *Proc. Natl. Acad. Sci. USA*, **1987**, *84*, 2565.

- [8] J.-M. Lehn, A. Rigault, *Angew. Chem. Int. Ed. Engl.* **1988**, 27, 1095.
- [9] D. Zurita, P. Baret, J.L. Pierre, *New J. Chem.* **1994**, 18, 1143.
- [10] C. Piguet, J.C. Bünzli, G. Bernardinelli, C.F. Bochet, P. Froidevaux, *J. Chem. Soc., Dalton Trans.* **1995**, 83.
- [11] A.T. Baker, D.C. Graig, G. Dong, *Inorg. Chem.* **1996**, 35, 1091.
- [12] A.K. Duhme, Z. Dauter, R.C. Hider, S. Pohl, *Inorg. Chem.* **1996**, 35, 3059.
- [13] E.J. Enemark, T.D.P. Stack, *Inorg. Chem.* **1996**, 35, 2719.
- [14] E.C. Constable, F. Heirtzler, M. Neuberger, M. Zehner, *J. Am. Chem. Soc.* **1997**, 119, 5606.
- [15] K.T. Potts, M.P. Wentland, D. Ganguly, G.D. Storrier, S.K. Cha, J. Cha, H.D. Abruña, *Inorg. Chim. Acta* **1999**, 288, 189.
- [16] S.M. Couchman, J.C. Jeffery, M.D. Ward, *Polyhedron* **1999**, 18, 2633.
- [17] P.N.W. Baxter, G.S. Hanan, J.M. Lehn, *J. Chem. Soc., Chem. Commun.* **1996**, 2019.
- [18] See for instance: M.-T. Youinou, N. Rahmouni, J. Fischer, J. A. Osborn, *Angew. Chem. Int. Ed. Engl.* **1992**, 31, 733; P. N. W. Baxter, J.-M. Lehn, J. Fischer, M.-T. Youinou, *Angew. Chem. Int. Ed. Engl.* **1994**, 33, 2284; A. M. Garcia, F. J. Romero-Salguero, D. M. Bassani, J.-M. Lehn, G. Baum, D. Fenske, *Chem. Eur. J.* **1999**, 5, 1803; G. S. Hanan, D. Volkmer, U. S. Schubert, J.-M. Lehn, G. Baum, D. Fenske, *Angew. Chem. Int. Ed. Engl.* **1997**, 36, 1842.
- [19] B. Hasenknopf, J.-M. Lehn, B.O. Kneisel, G. Baum, D. Fenske, *Angew. Chem. Int. Ed. Engl.* **1996**, 35, 1838; B. Hasenknopf, J.-M. Lehn, N. Boumediene, A. Dupont-Gervais, A. Van Dorsselaer, B. Kneisel, D. Fenske, *J. Am. Chem. Soc.* **1997**, 119, 10956.
- [20] P.N.W. Baxter, J.M. Lehn, A. De Cian, J. Fischer, *Angew. Chem. Int. Ed. Engl.* **1993**, 32, 69; P. N. W. Baxter, J.-M. Lehn, G. Baum, D. Fenske, *Chem. Eur. J.* **1999**, 5, 102;

- P. N. W. Baxter, J.-M. Lehn, B. O. Kneisel, G. Baum, D. Fenske, *Chem. Eur. J.* **1999**, *5*, 113.
- [21] C. O. Dietrich-Buchecker, J. P. Sauvage, *Bioorg. Chem. Front.*, Dugas, H., Ed., Springer-Verlag, Berlin, 1991, Vol. 2, p. 146.
- [22] J.C. Chambron, C.O. Dietrich-Buchecker, J.P. Sauvage, in 'Comprehensive Supramolecular Chemistry', Eds. J. P. Sauvage, M.W. Hosseini, Pergamon, Oxford, 1996, Vol.9, Chapter 2, p. 43.
- [23] D.B. Amabilino, J.F. Stoddart, *Chem. Rev.* **1995**, *95*, 2725.
- [24] B. Hasenknopf, J.-M. Lehn, *Helv. Chim. Acta* **1996**, *79*, 1643.
- [25] R. Krämer, J.-M. Lehn, A. DeCian, J. Fischer, *Angew. Chem. Int. Ed. Engl.* **1993**, *32*, 703.
- [26] C. Piguet, G. Hopfgartner, B. Bocquet, O. Schaad, A.F. Williams, *J. Am. Chem. Soc.* **1994**, *116*, 9092; V. C. M. Smith, J.-M. Lehn, *Chem. Commun.* **1996**, 2733.
- [27] B. Hasenknopf, J.-M. Lehn, G. Baum, D. Fenske, *Proc. Natl. Acad. Sci. USA* **1996**, *93*, 1397.
- [28] V.A. Grillo, E.J. Seddon, C.M. Grant, G. Aromi, J.C. Bollinger, K. Folting, G. Christou, *Chem. Commun.* **1997**, 1561; W. Dai, H. Hu, X. Wei, S. Zhu, D. Wang, K. Yu, K. Dalley, X. Kou, *Polyhedron* **1997**, *16*, 2059; C. Piguet, G. Hopfgartner, B. Bocquet, O. Schaad, A.F. Williams, *J. Am. Chem. Soc.* **1994**, *116*, 9092.
- [29] D.P. Funeriu, Y.B. He, H.J. Bister, J.M. Lehn, *Bull. Soc. Chim. Fr.* **1996**, *133*, 673; B. Kersting, M. Meyer, R.E. Powers, K.N. Raymond, *J. Am. Chem. Soc.* **1996**, *30*, 7221.
- [30] M. Jaquinod, E. Leize, N. Potier, A.M. Albrecht, A. Shanzer, A. Van Dorsselaer, *Tetrahedron Lett.* **1993**, *34*, 2771; G. Hopfgartner, C. Piguet, J.D. Henion, A.F. Williams, *Helv. Chim. Acta* **1993**, *76*, 1759; G. Hopfgartner, C. Piguet, J.D. Henion, *J. Am. Soc. Mass Spectrom.* **1994**, 748.

- [31] G. Hopfgartner, C. Piguet, J.D. Henion, A.F. Williams, *Helv. Chim. Acta* **1993**, *76*, 1759.
- [32] M. Greenwald, M. Eassa, E. Katz, I. Willner, Y. Cohen, *J. Electroanal. Chem.* **1997**, *434*, 77.
- [33] A. Marquis-Rigault, A. Dupont-Gervais, P.N.W. Baxter, A. Van Dorsselaer, J.M. Lehn, *Inorg. Chem.* **1996**, *35*, 2307.
- [34] C. Piguet, G. Bernardinelli, B. Bocquet, A. Quattropiani, A.F. Williams, *J. Am. Chem. Soc.* **1992**, *114*, 7440.
- [35] C. Piguet, J.C. Bünzli, G. Bernardinelli, C.G. Bochet, P. Froidevaux, *J. Chem. Soc. Dalton Trans.* **1995**, 83; S. Petoud, J.C. Bünzli, F. Renaud, C. Piguet, K.J. Schenk, G. Hopfgartner, *Inorg. Chem.* **1997**, *36*, 5750.
- [36] A. Pfeil, J.M. Lehn, *J. Chem. Soc., Chem. Commun.* **1992**, 838.
- [37] T.M. Garrett, U. Koert, J.M. Lehn, *J. Phys. Org. Chem.* **1992**, *5*, 529.
- [38] S. Blanc, P. Yakirevitch, E. Leize, M. Meyer, J. Libman, A. Van Dorsselaer, A.M. Albrecht-Gary, A. Shanzer, *J. Am. Chem. Soc.* **1997**, *119*, 4934.
- [39] A. Marquis-Rigault, A. Dupont-Gervais, A. Van Dorsselaer, J.M. Lehn, *Chem. Eur. J.* **1996**, *2*, 1395.
- [40] N. Fatin-Rouge, S. Blanc, E. Leize, A. Van Dorsselaer, P. Baret, J.-L. Pierre, Albrecht-Gary, *Inorg. Chem.* **2000**, *39*, 5771.
- [41] M.M. Harding, U. Koert, J.M. Lehn, A. Marquis-Rigault, C. Piguet, J. Siegel, *Helv. Chim. Acta* **1991**, *74*, 594.
- [42] R. Krämer, J.M. Lehn, A. Marquis-Rigault, *Proc. Natl. Acad. Sci. USA* **1993**, *90*, 5394.
- [43] H. Meerwein, V. Hederich, K. Wunderlich, *Ber. Deutsch. Pharm. Ges.* **1958**, *63*, 548.
- [44] L.G. Sillen, *Acta Chem. Scand.* **1964**, *18*, 1085.
- [45] L.G. Sillen, B. Warnqvist, *Ark. Kemi.* **1968**, *31*, 377.

- [46] J. Havel, *Pure Appl. Chem.* **1972**, *34*, 370.
- [47] H. Gampp, M. Maeder, C.J. Meyer, A.D. Zuberbühler, *Talanta* **1985**, *32*, 95.
- [48] F.J.C. Rossoti, H.S. Rossoti, R.J. Whewell, *J. Inorg. Nucl. Chem.* **1971**, *33*, 2051.
- [49] H. Gampp, M. Maeder, C.J. Meyer, A.D. Zuberbühler, *Talanta* **1985**, *32*, 257.
- [50] H. Gampp, M. Maeder, C.J. Meyer, A.D. Zuberbühler, *Talanta* **1986**, *33*, 943.
- [51] D.W. Marquardt, *J. Soc. Indust. Appl. Math.* **1963**, *11*, 431.
- [52] M. Maeder, A.D. Zuberbühler, *Anal. Chem.* **1990**, *62*, 2220.
- [53] Bio-Logic Company, Ed. Bio-Logic Company, Echirolles, **1991**.
- [54] J.A. Nelder, R. Mead, *The Computer Journal* **1965**, *7*, 308.
- [55] E. Yeramian, P. Claverie, *Nature* **1987**, *326*, 169.
- [56] J. Leatherbarrow, Ed. Biosoft, Cambridge, **1987**.
- [57] N. Ingri, W. Kakolowicz, L.G. Sillen, B. Warnqvist, *Talanta* **1967**, *14*, 1261.
- [58] R.J.P. Williams, *J. Chem Soc.* **1955**, 137.
- [59] R.A. Palmer, T.S. Piper, *Inorg. Chem.* **1966**, *5*, 864.
- [60] W.R. McWinnie, J.D. Miller, *Adv. Inorg. Chem. Radiochem.* **1969**, *12*, 135.
- [61] S. Kitakawa, M. Munakata, A. Hitgashie, *Inorg. Chim. Acta* **1984**, *5*, 79.
- [62] S. Kitakawa, M. Munakata, A. Hitgashie, *Inorg. Chim. Acta* **1982**, *59*, 219.
- [63] C.C. Phiher, D.R. McMillin, *Inorg. Chem.* **1986**, *5*, 1329.
- [64] C.S. Tsai, *Can. J. Chem.* **1967**, *45*, 2862.
- [65] E. Muller, C. Piguet, G. Bernardinelli, A.F. Williams, *Inorg. Chem.* **1988**, *27*, 849.
- [66] A. Rigault, Ph.D. Thesis, Université Louis Pasteur de Strasbourg, France, **1992**.
- [67] U. Ochsenbein, Ph.D. Thesis, Université de Fribourg, Switzerland, **1981**.
- [68] J. Lange, H. Elias, H. Paulus, J. Muller, U. Weser, *Inorg. Chem.* **2000**, *39*, 3342.
- [69] W. Zarges, J. Hall, J.M. Lehn, *Helv. Chim. Acta* **1991**, *74*, 1843.

- [70] B. Hasenknopf, J.M. Lehn, N. Boumediene, M. Leize, A. Van Dorsselaer, *Angew. Chem. Int. Ed.* **1998**, *37*, 3265
- [71] P. Leupin, Ph.D. Thesis, Université de Fribourg, Switzerland, **1980**.
- [72] E.I. Onstott, H.A. Laitinen, *J. Chem. Soc.* **1950**, 4724.
- [73] B.R. James, J.P. Williams, *J. Chem. Soc.* **1961**, 2007.
- [74] G. Anderreg, *Helv. Chim. Acta* **1963**, *46*, 2397.
- [75] A. Pfeil, J.M. Lehn, unpublished results.
- [76] B.R. James, M. Parris, J.P. Williams, *J. Chem. Soc.* **1961**, 4630.

Captions to Figures

Fig. 1. Structure of ligands **L** ($X = \text{CON}(\text{Et})_2$) [40] and **L'** ($X = \text{CO}_2\text{Et}$) [42].

Fig. 2. Electrospray mass spectra. a) $[\text{Cu}(\text{I})]_{\text{tot}}/[\text{L}]_{\text{tot}} = 0.1$; b) 0.5; c) 1.0; d) 20; positive mode $[\text{L}]_{\text{tot}} = 1.2 \times 10^{-4} \text{ M}$; Solvent: $\text{CH}_3\text{CN}:\text{H}_2\text{O}:\text{CH}_2\text{Cl}_2$, (80:15:5).

Fig. 3. Absorption spectra of **L** with varying copper(I) concentrations. Solvent: $\text{CH}_3\text{CN}/\text{H}_2\text{O}/\text{CH}_2\text{Cl}_2$, 80/15/5 v/v; $T = 25.0$ (2) $^\circ\text{C}$; $I = 0.1$; a) $l = 0.2 \text{ cm}$; b) $l = 1 \text{ cm}$; $[\text{L}]_{\text{tot}} = 1.2 \times 10^{-4} \text{ M}$; 1-24: $[\text{Cu}(\text{I})]_{\text{tot}} \times 10^5 \text{ M} = 0; 1.2; 2.4; 3.6; 4.8; 6.0; 7.2; 8.4; 9.6; 10.8; 12.0; 13.2; 14.4; 15.6; 16.8; 18.0; 19.2; 20.4; 21.6; 22.8; 24; 59.9; 119.9; 240.0 \text{ M}$ respectively.

Fig. 4. Distribution curves related to the formation of cuprous complexes with **L**. (a) $[\text{L}]_{\text{tot}} = 10^{-4} \text{ M}$, (b) $[\text{L}]_{\text{tot}} = 2.5 \times 10^{-5} \text{ M}$, and with **L'** (c) $[\text{Cu}(\text{I})]_{\text{tot}} = 5.7 \times 10^{-6} \text{ M}$. Solvent: $\text{CH}_3\text{CN}/\text{H}_2\text{O}/\text{CH}_2\text{Cl}_2$, 80/15/5 v/v except for (c) $\text{CH}_3\text{CN}/\text{CH}_2\text{Cl}_2$ 50/50 v/v; $T = 25.0 \text{ }^\circ\text{C}$; $I = 0.1$; the stability constants are given in Table 1.

Fig. 5. Evolution of the absorption observed for the formation kinetics of the cuprous complexes with **L** versus time. Solvent: $\text{CH}_3\text{CN}/\text{H}_2\text{O}/\text{CH}_2\text{Cl}_2$, 80/15/5 v/v; $T = 25.0$ (2) $^\circ\text{C}$; $I = 0.1$; $[\text{L}]_{\text{tot}} = 2.5 \times 10^{-5} \text{ M}$; $[\text{Cu}(\text{I})]_{\text{tot}} = 3.1 \times 10^{-4} \text{ M}$; $l = 1 \text{ cm}$; $\lambda = 468 \text{ nm}$.

Fig. 6. Time-resolved electronic spectra recorded for the formation of **L** copper(I) complexes. Solvent: $\text{CH}_3\text{CN}/\text{H}_2\text{O}/\text{CH}_2\text{Cl}_2$, 80/15/5 v/v; $T = 25.0$ (2) $^\circ\text{C}$; $I = 0.1$; $[\text{L}]_{\text{tot}} = 2.5 \times 10^{-5} \times \text{M}$; $l = 1 \text{ cm}$; $[\text{L}] = 2.5 \times 10^{-5} \text{ M}$; $[\text{Cu}(\text{I})] = 2.5 \times 10^{-4} \text{ M}$; $t_1 = 2.5 \text{ ms}$ and $t_4 = 500 \text{ s}$.

Fig. 7. Variation of the (a) first, (b) second and (c) third pseudo-first order constants for the formation of **L** cuprous complexes versus the concentrations of the Cu(I) reacting species.

Solvent: $\text{CH}_3\text{CN}/\text{H}_2\text{O}/\text{CH}_2\text{Cl}_2$, 80/15/5 v/v; $T = 25.0$ (2) $^\circ\text{C}$; $I = 0.1$; $[\text{L}]_{\text{tot}} = 2.5 \times 10^{-5} \text{ M}$.

Fig. 8. Schematic representation of **L** cuprous complexes.

Fig. 9. Schematic representation of the proposed mechanism.

Table 1. Global Stability Constants and Spectrophotometric Parameters for the Cuprous Complexes Formed with L^a and L'^b

Equilibrium	$\log \beta (3\sigma)$	λ_{\max} nm	ϵ_{\max} $M^{-1} \text{ cm}^{-1}$
$L + \text{Cu(I)} \rightleftharpoons \text{LCu}$	$\log \beta_{\text{LCu}} = 4.2 (1)$	468	6800
$2 L + 2\text{Cu(I)} \rightleftharpoons \text{L}_2\text{Cu}_2$	$\log \beta_{\text{L}_2\text{Cu}_2} = 12.9 (3)$	468	14000
$2 L + 3 \text{Cu(I)} \rightleftharpoons \text{L}_2\text{Cu}_3$	$\log \beta_{\text{L}_2\text{Cu}_3} = 18.7 (3)$	468	17000
$L' + \text{Cu(I)} \rightleftharpoons \text{L}'\text{Cu}$	$\log \beta_{\text{L}'\text{Cu}} = 4.6 (2)$	500	7700
$2 L' + \text{Cu(I)} \rightleftharpoons \text{L}'_2\text{Cu}$	$\log \beta_{\text{L}'_2\text{Cu}} = 8.2 (2)$	500	8500
$2 L' + 2\text{Cu(I)} \rightleftharpoons \text{L}'_2\text{Cu}_2$	$\log \beta_{\text{L}'_2\text{Cu}_2} = 13.5 (2)$	500	16000
$2 L' + 3 \text{Cu(I)} \rightleftharpoons \text{L}'_2\text{Cu}_3$	$\log \beta_{\text{L}'_2\text{Cu}_3} = 18.6 (1)$	500	26000

^aSolvent: $\text{CH}_3\text{CN}/\text{H}_2\text{O}/\text{CH}_2\text{Cl}_2$, 80/15/5 v/v; $T = 25.0 (2) \text{ }^\circ\text{C}$; $I = 0.1$; ^bsolvent:

$\text{CH}_3\text{CN}/\text{CH}_2\text{Cl}_2$, 50/50 v/v; ref. 36. The errors are estimated to 1 nm for the wavelengths and to 5% for the extinction coefficients. For the sake of simplicity charges have been omitted in all the chemical equilibria.

Table 2. Kinetic and Thermodynamic Parameters Determined for the Formation of Cu(I) Complexes of L^a and L^b

Rate limiting step		Kinetic results
Step 1		
$L + Cu \xrightleftharpoons{\beta_{LCu^*}} LCu$	L	$\log \beta_{LCu^*} = 3.6$ (4) $\log \beta_{LCu_2^*} = 8.1$ (3)
$LCu^* + Cu \xrightleftharpoons{K_{LCu_2^*}} LCu_2^*$	L'	$\log \beta_{L'Cu^*} = 4.0$ (5) $\log \beta_{L'Cu_2^*} = 8.0$ (5)
Step 2		
$LCu_2^* + L \xrightleftharpoons[k_{-2}]{k_2} L_2Cu_2^*$	L	$k_2 = 7$ (3) $\times 10^5 M^{-1} s^{-1}$ $k_{-2} = 53.0$ (6) s^{-1} $\Rightarrow \log \beta_{L_2Cu_2^*} = 12.2$ (6)
	L'	$k_2 = 2.0$ (7) $\times 10^5 M^{-1} s^{-1}$ $k_{-2} = 0.6$ (2) s^{-1} $\Rightarrow \log \beta_{L'_2Cu_2^*} = 13.5$ (6)
Step 3		
$L_2Cu_2^* + Cu \xrightleftharpoons[k_{-3}]{k_3} L_2Cu_3^*$	L	$k_3 = 1.0$ (1) $\times 10^3 M^{-1} s^{-1}$ $k_{-3} = 7.2$ (4) $\times 10^{-2} s^{-1}$ $\Rightarrow \log \beta_{L_2Cu_3^*} = 16.9$ (8)
	L'	$k_3 = 45$ (9) $M^{-1} s^{-1}$ $k_{-3} = 9$ (2) $\times 10^{-2} s^{-1}$ $\Rightarrow \log \beta_{L'_2Cu_3^*} = 16.2$ (8)
Step 4		
$L_2Cu_3^* \xrightleftharpoons[k_{-4}]{k_4} L_2Cu_3$	L	$k_4 = 2.0$ (4) $\times 10^{-2} s^{-1}$ $k_{-4} = 1.1$ (2) $\times 10^{-2} s^{-1}$ $\Rightarrow \log \beta_{L_2Cu_3} = 17$ (1)
	L'	$k_4 = 3$ (2) $\times 10^{-2} s^{-1}$ $k_{-4} = 2.7$ (2) $\times 10^{-2} s^{-1}$ $\Rightarrow \log \beta_{L'_2Cu_3} = 16.3$ (9)
$L'Cu^* + L' \xrightleftharpoons[k_{-1}]{k_1} L'_2Cu$		$k_1 = 1.7$ (9) $\times 10^3 M^{-1} s^{-1}$ $k_{-1} = 0.22$ (7) s^{-1} $\Rightarrow \log k_1/k_{-1} = 3.9$ (5)

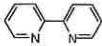
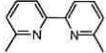
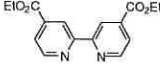
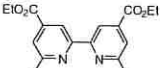
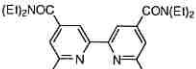
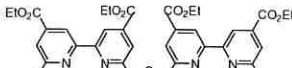
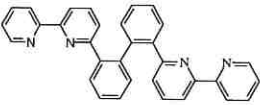
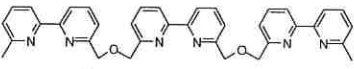
^aSolvent: CH₃CN/H₂O/CH₂Cl₂, 80/15/5 v/v; $T = 25.0$ (2) °C; $I = 0.1$; ^b Solvent: CH₃CN/CH₂Cl₂, 1/1 v/v; $T = 25.0$ (2) °C; $I = 0.1$. The errors are given as 3σ .

Table 3. Variation of the Pseudo-First Order Constants and the Absorbance for the Formation of the Cuprous Complexes of L' versus $[Cu(I)]^a$

$[L']_{tot} \times 10^5$ (M)	$[Cu(I)]_{tot} \times 10^3$ (M)	$k_{2,obs}$ (s^{-1})	$k_{3,obs}$ (s^{-1})	$k_{4,obs}$ (s^{-1})	$A_{2,0}$	$A_{2,\infty}$
2.9	0.423	-	0.12	0.033	0.1	-
2.9	0.546	1.297	0.105	0.029	0.1	-
2.9	0.706	1.223	-	-	0.11	-
6.5	0.908	-	0.125	0.032	-	-
5.2	1.539	-	0.117	0.031	-	0.338
8.5	2.000	0.698	0.152	0.036	0.34	0.57
12.2	2.234	0.723	0.154	0.036	-	0.331
6.5	2.269	0.601	0.138	0.038	0.205	-
8.5	4.000	0.773	-	-	0.3	-
6.5	4.539	0.638	-	-	0.2	-
6.5	9.077	0.932	-	-	0.18	0.242
8.5	10.000	0.795	-	-	-	-

^aSolvent: CH_3CN/CH_2Cl_2 , 50/50 v/v; $T = 25.0$ (2) $^{\circ}C$; $I = 0.1$; $l = 1$ cm; $\lambda = 500$ nm.

Table 4. Global Stability Constants of Cu(I) Complexes with Various Bipyridine Ligands.

Ligand	$\log \beta$	λ_{\max} (nm) { ϵ_{\max} ($M^{-1} \text{ cm}^{-1}$)}	Solvent
 1	$\log \beta_{\text{LCu}} = 3.90$ $\log \beta_{\text{L}_2\text{Cu}} = 6.8(1)$ $12.95 < \log \beta_{\text{L}_2\text{Cu}} < 14.2$	341 {2240} 438 {5200}	CH_3CN [71] H_2O [72-74]
 2	$\log \beta_{\text{LCu}} = 5.4$ $\log \beta_{\text{L}_2\text{Cu}} = 10.2$ $\log \beta_{\text{LCu}} = 3.8$ $\log \beta_{\text{L}_2\text{Cu}} = 9.3$ $\log \beta_{\text{L}_2\text{Cu}} = 15.8$	345 {2100} 440 {5000} 450 {6140} - 455 {5570} 455 {6570}	CH_3CN [67] $\text{CH}_3\text{CN}/\text{CH}_2\text{Cl}_2$ 50/50 [75] $\text{H}_2\text{O}/\text{CH}_2\text{Cl}_2$ 50/50 [73,76]
 3	$\log \beta_{\text{L}_2\text{Cu}} = 11.4$	483 {7130}	$\text{H}_2\text{O}/\text{CH}_2\text{Cl}_2$ 50/50 [73,76]
 4	$\log \beta_{\text{LCu}} = 4.5$ $\log \beta_{\text{L}_2\text{Cu}} = 8.6$	380 {3380} 500 {10750}	$\text{CH}_3\text{CN}/\text{CH}_2\text{Cl}_2$ 50/50 [75]
 5		470 {7100}	$\text{CH}_3\text{CN}/\text{CH}_2\text{Cl}_2$ 50/50 [66]
 6	$\log \beta_{\text{L}_2\text{Cu}_2} = 14$	500 {15400}	$\text{CH}_3\text{CN}/\text{CH}_2\text{Cl}_2$ 50/50 [75]
 7	$\log \beta_{\text{LCu}} = 6.9$	465 {4400} 533 {1600}	CH_3CN [65]
 8	$\log \beta_{\text{L}_2\text{Cu}_3} = 20.0$	450 {15260}	$\text{CH}_3\text{CN}/\text{CH}_2\text{Cl}_2$ 50/50 [75]

Mixed solvent ratio expressed by volume (v/v).

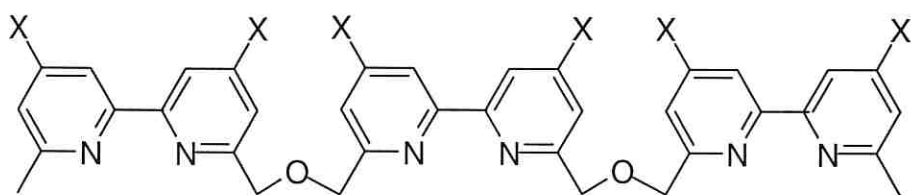
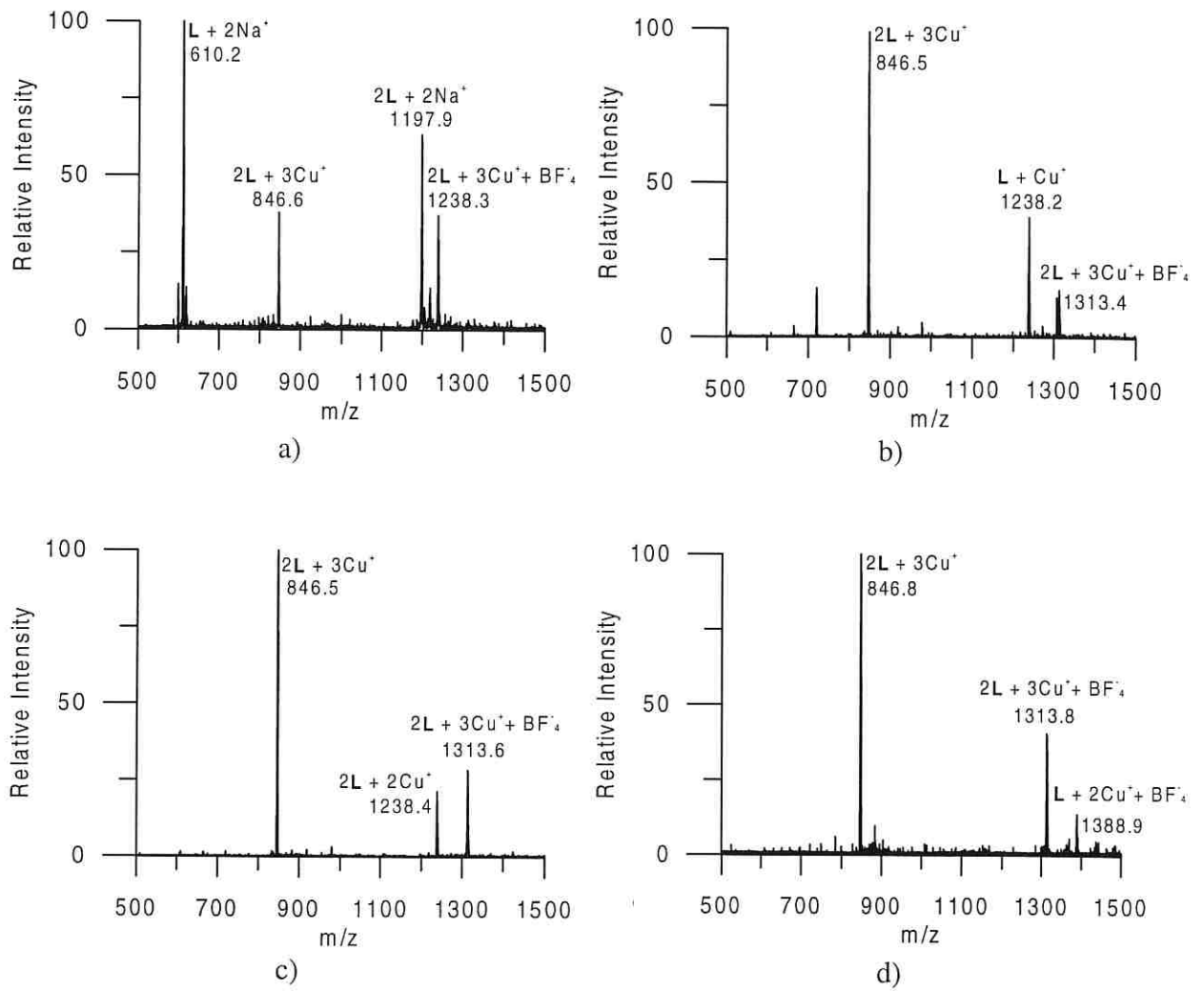
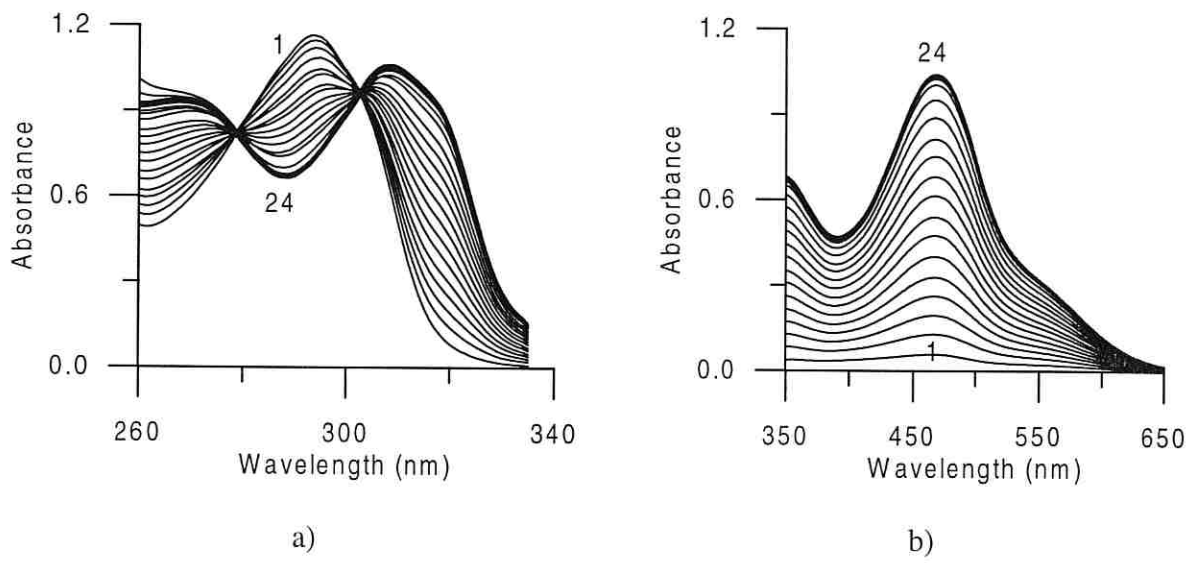
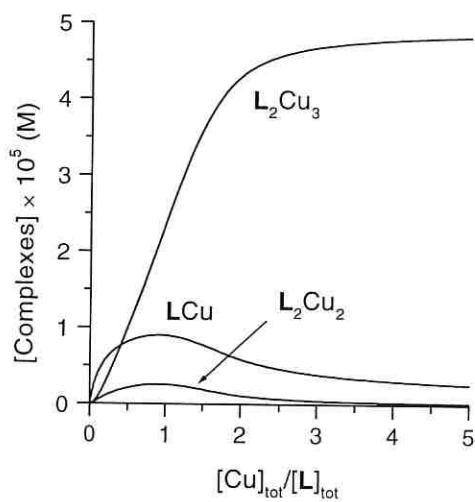


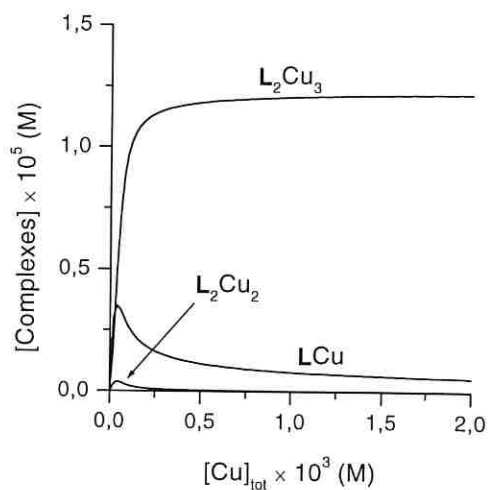
Fig. 1

*Fig. 2*

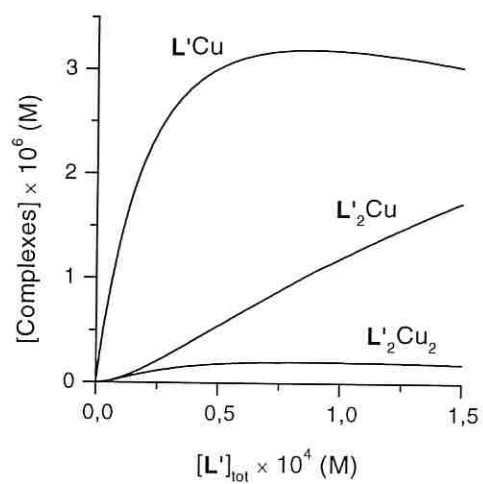
*Fig. 3*



a)

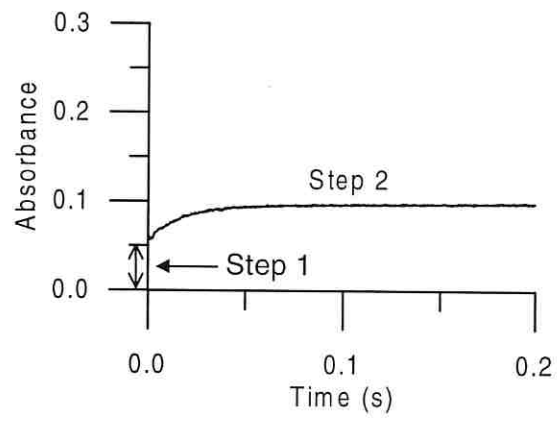


b)

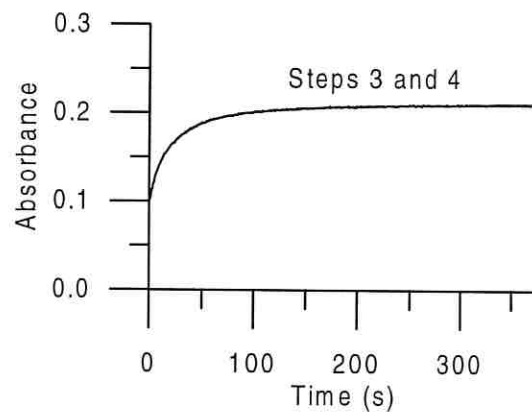


c)

Fig. 4

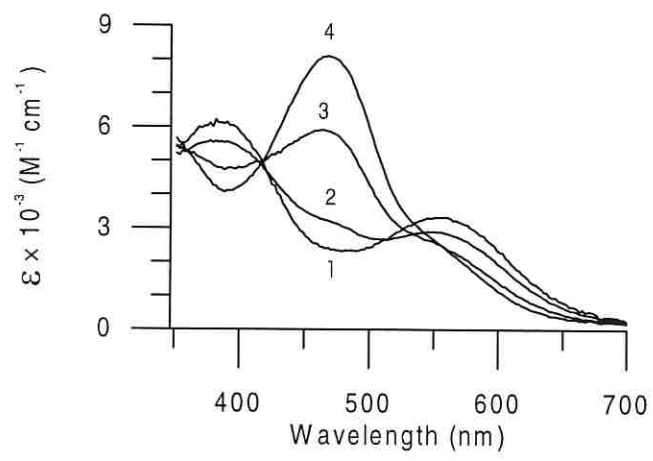


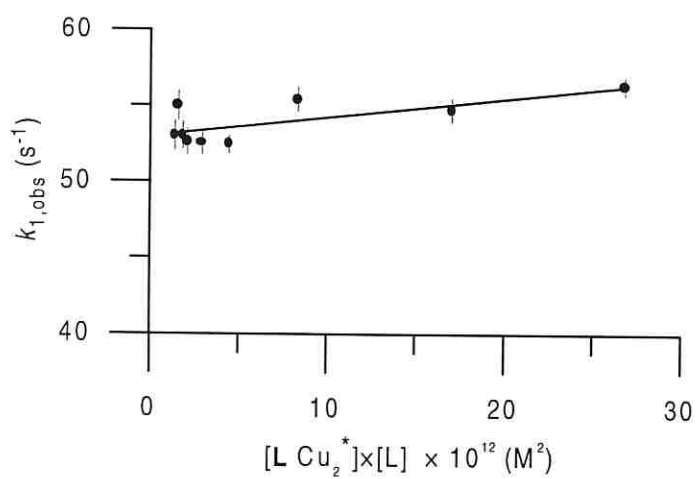
a)



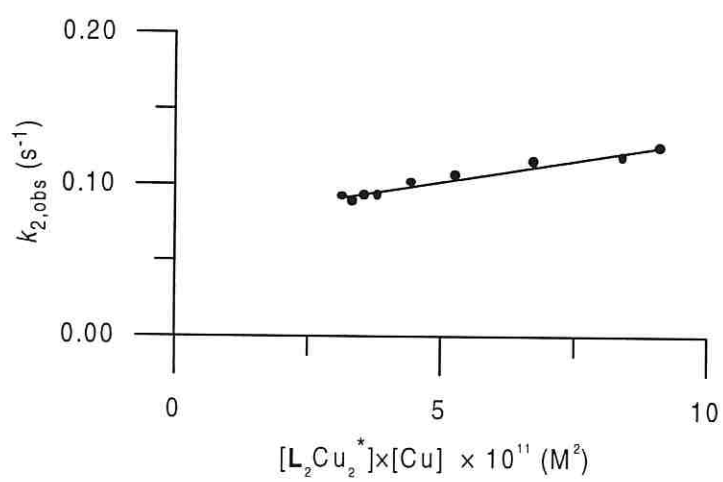
b)

Fig. 5

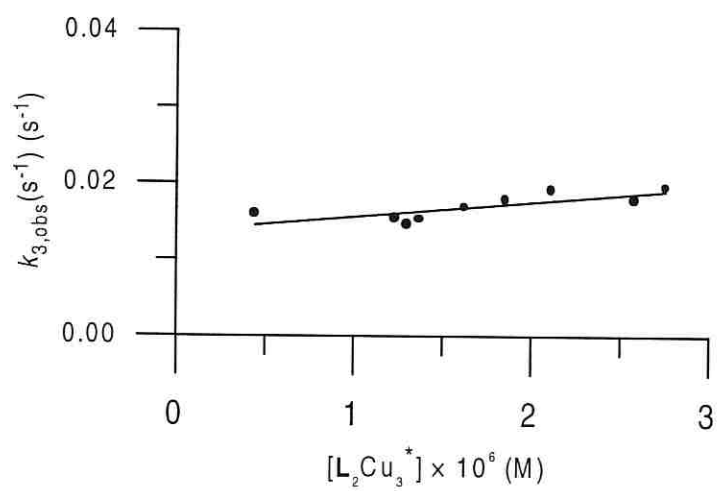
*Fig. 6*



a)

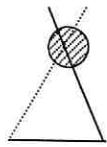


b)

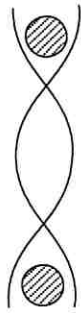


c)

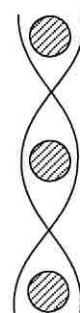
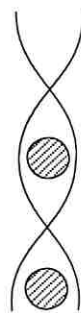
Fig. 7



LCu



L_2Cu_2



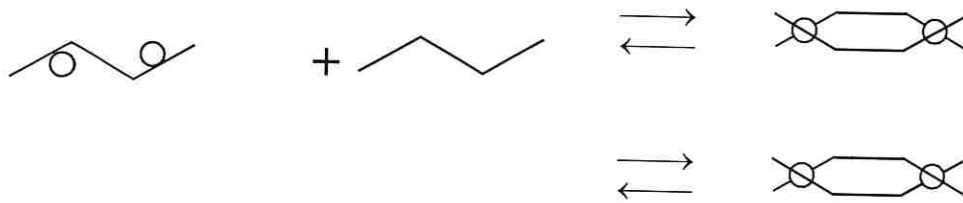
L_2Cu_3

Fig. 8

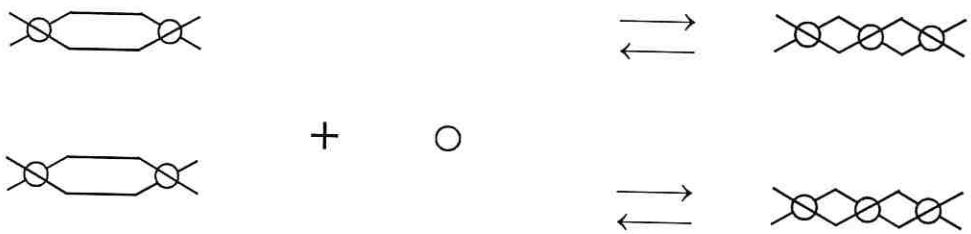
Step 1



Step 2



Step 3



Step 4

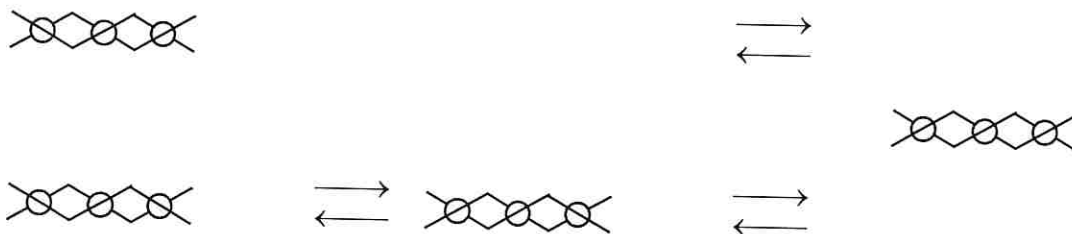


Fig. 9